Time-resolved x-ray diffraction reveals multiple conformations in the M–N transition of the bacteriorhodopsin photocycle

Toshihiko Oka*†, Naoto Yagi‡, Tetsuro Fujisawa†, Hironari Kamikubo§, Fumio Tokunaga*, and Mikio Kataoka¶‖

*Department of Earth and Space Science, Graduate School of Science, Osaka University, Toyonaka, Osaka 560-0043, Japan; †Institute of Physical and Chemical Research (RIKEN) Harima Institute/SPring-8, Mikazuki, Sayo, Hyogo 679-5148, Japan; ‡Experimental Division, Japan Synchrotron Radiation Research Institute (JASRI), Mikazuki, Sayo, Hyogo 679-5198, Japan; §Structural Biophysics Laboratory, Institute of Materials Structure Science, High Energy Accelerator Research Organization, Tsukuba, Ibaraki 305-0801, Japan; and ¶Graduate School of Materials Science, Nara Institute of Science and Technology, Ikoma, Nara 630-0101, Japan

Communicated by Yasuyuki Yamada, Nara Institute of Science and Technology, Nara, Japan, October 24, 2000 (received for review August 21, 2000)

We measured the M–N transition of wild-type bacteriorhodopsin (pH 9, 10°C) by time-resolved x-ray diffraction study at SPring8 BL45XU-A. We confirmed the accumulation of M and N intermediates by absorbance measurements, and we found that the time resolution of x-ray diffraction experiments (244 ms) was sufficient to resolve the M–N transition. From the x-ray diffraction data, three components were decomposed by singular value decomposition analysis. The existence of three components in the M→N→BR reaction revealed that BR changes its structure during the M–N transition. Moreover, the difference Fourier maps of reconstituted fast and slow decay components clearly showed that the electron density distributions of the F helix changes in the M–N transition. The observed structural change at the F helix will increase access of the Schiff base and D96 to the cytoplasmic surface and facilitate the proton transfer steps that begin with the decay of the M state.

An ion pump protein transports ions across the membrane against the chemical potential. A simple idea of the ion pumping mechanism is that the ion-binding states of the ion pump are linked to protein conformations to switch the ion transport pathway from one membrane surface to another surface (1). Bacteriorhodopsin (BR) is one of the proton transport proteins that make use of absorbed photon energy. Its photocycle is characterized by distinct spectra of the metastable intermediate in the visible range as J, K, L, M, N, and O. The most important steps for the proton pump are deprotonation and reprotonation of the Schiff base. The former is the proton transfer from the Schiff base to D85 and the latter is the proton transfer from D96 to the Schiff base. Proton transfer from the Schiff base to D85 occurs in the L–M transition. The structure of the M intermediate was investigated by diffraction methods under stabilizing conditions (2–4). The obtained data showed that the structure of the M intermediate differed largely from the unphotolyzed state. It was shown that this structural change is closely related to the deprotonation of the Schiff base; in the original structure (conformation E) the proton channel is open to the extracellular side, and when an M-type conformation is assumed (conformation C), it is open to the cytoplasmic side (5–7). This structural transition after the first proton transfer prevents reverse proton transfer from D85 to the Schiff base. Thus, the alternating protein conformation model explains the proton transport mechanism (7). The Schiff base is reprotonated from D96 during the M–N transition. Because D96 is located in a hydrophobic environment, it has unusual high pK and it is protonated in an unphotolyzed state. The pK of D96 should be lowered during the M–N transition to transfer a proton. Therefore, an important event in lowering the D96 pK is expected to occur at the M–N transition.

Structural studies on photointermediates have been carried out by accumulating specific intermediates using chemical treatments (3, 4), mutations (8, 9), or quenching methods (4, 10). However, a structural study during the real photocycle is necessary to confirm that the intermediate structures observed so far are not artifacts of the chemical treatments or mutations. For this purpose, time-resolved x-ray diffraction experiments under a near physiological condition have been tried by using laser plasma x-ray (11) and synchrotron radiation (8). The former work was, however, only a feasibility study and gave no useful information on the intermediate. The latter work was a study on the structural kinetics of BR by x-ray diffraction. The authors of the latter report estimated the time constant of the decay process of the D96N M intermediate through the time course of the intensity change of a specific reflection. Time-resolved diffraction experiments have some difficulties from technical viewpoints, particularly in their lack of incident x-ray intensity, lack of sufficient readout speed of a detector, and lack of the detecting efficiency of a detector. Moreover, extraction of components existing in the photocycle and determination of their time courses are required, because the states observed by time-resolved experiments are mixtures of several photointermediates. The diffraction profile and the time course should be analyzed simultaneously with the time-resolved x-ray diffraction data.

We carried out time-resolved x-ray diffraction experiments on purple membranes by using a third-generation synchrotron radiation source, SPring-8, with a charge-coupled device (CCD) detector. A CCD x-ray detector is now commonly used as a two-dimensional detector instead of an imaging plate. One advantage of the CCD detector is its fast readout speed. The CCD detector we used can read one frame picture (656×496 pixels) every 36 ms. Time-resolved diffraction data recorded with this detector was analyzed by the singular value decomposition (SVD) method. The SVD method can enable extraction of information contained in a data set efficiently with a minimum number of input assumptions (12). From the SVD analysis, we were able to determine the number of components, the diffraction profile, and the time course of each component. We found that the decay kinetics of the M and N intermediates of wild-type BR is composed of at least two different components. The difference Fourier maps of the two components reconstituted from the time-resolved diffraction data show the changes characteristic to the M and the N intermediates, respectively. The present results suggests that the decay of the M intermediate is

Abbreviations: BR, bacteriorhodopsin; SVD, singular value decomposition; CCD, charge-coupled device.

‖To whom reprint requests should be addressed. E-mail: kataoka@ms.aist-nara.ac.jp.

The publication costs of this article were defrayed in part by page charge payment. This article must therefore be hereby marked "*advertisement*" in accordance with 18 U.S.C. §1734 solely to indicate this fact.

Article published online before print: *Proc. Natl. Acad. Sci. USA*, 10.1073/pnas.260504897. Article and publication date are at www.pnas.org/cgi/doi/10.1073/pnas.260504897

followed by the decay of the N intermediate and that there are small, but meaningful, structural differences between the M and the N intermediates. We conclude that BR uses a two-step large structural change in proton pumping.

Materials and Methods

Samples. Purple membrane sheets of wild-type BR were isolated by the standard method (13), and purple membrane sheets were suspended in 20 mM of Tris buffer (pH 9). A 20-μl drop of suspension was dried on a piece of mylar sheet, and another drop was layered onto the resulting wet film. The layering procedure was repeated three times for x-ray diffraction experiments and one time for optical measurements. The film was incubated at 25°C and 95% relative humidity for 1 day.

Absorbance Measurements. Flash-induced absorbance changes at 410 nm and 570 nm of wild-type BR were measured to confirm the deprotonation and reprotonation of the Schiff base as follows. The sample was placed between a reference halogen lamp (Mega Light 100, Hoya-Schott, Tokyo) and a monochromator (SPG-120S, Shimadzu) with a photomultiplier (R928-09, Hamamatsu Photonics, Hamamatsu City, Japan). An ADC card (REX5054, RATOC System Inc., Osaka) connected to a notebook computer (Toshiba, Tokyo) recorded output signals. The samples were excited with a xenon flash lamp with Toshiba Y50 and C50D filters ($500 < \lambda < 630$ nm). Temperature was kept at 10°C during the measurements. The time resolution of the measurements was 10 ms.

Time-Resolved X-Ray Diffraction. Time-resolved x-ray diffraction experiments were carried out at the RIKEN Beamline I in SPring-8 (14). X-ray diffraction patterns up to 7 $Å^{-1}$ were recorded by a CCD camera (C4880–82, Hamamatsu Photonics) coupled with a 6-inch Hamamatsu Photonics x-ray image intensifier (14, 15). Two hundred frames were recorded with 244 ms time resolution. Temperature was kept at 10°C. The samples were excited by a xenon flash lamp with Toshiba Y50 and C50D filters ($500 < \lambda < 630$ nm) at 2.44 sec after the start of the diffraction measurement, which corresponds to the beginning of the 11th time frame.

Data Treatment. A series of sequential two-dimensional ring diffraction patterns were averaged circularly to reduce them into a set of sequential one-dimensional patterns, and 10 different data sets were averaged. The sequential one-dimensional diffraction patterns are equivalent to an m × n matrix, **A**, whose element is the diffraction intensity at the mth point of s ($=2\sin\theta/\lambda$) and the nth time point. The data were analyzed by the SVD method (for details, see ref. 12). The data matrix, **A**, can be described by an m × n matrix, **E**(s), and an n × n matrix, **C**(t), as

$$\mathbf{A}(s, t) = \mathbf{E}(s)\mathbf{C}(t) = \mathbf{USV}^{T}.$$

E(s) describes the diffraction pattern of the independent components, and **C**(t) describes their concentrations as a function of time t. The m × n matrix **U** contains the orthonormal basis spectra of diffraction pattern, the n × n diagonal matrix **S** contains the associated eigenvalues, and the n × n matrix **V** contains the time dependence of the basis spectra.

We consider the statistical weights for the data set **A.** The error of the data element $\mathbf{A}(s_i,t_j)$ is described as σ_{ij}, and $\mathbf{\Sigma}$ is the matrix of σ_{ij}. The error of data **A** depends on s but not on time because the measurement time slice is identical for all data and the intensity change is not so large. The value of σ_{ij} is given as the average of $\sqrt{\mathbf{A}_{ij}}$ for all frames (j = 1 to n), where $\sigma_{ij} = \sigma_{ik}$ (i, j, k: arbitrary index).

The weight matrix **B** is defined as $\mathbf{B}_{ij} = 1/\sigma_{ij}$ (i = j) and $\mathbf{B}_{ij} = 0$ ($i \neq j$).

According to above definition, $[\mathbf{B\Sigma}]_{ij} = 1$.

Therefore, the final data set to be analyzed should be **BA** as

$$\mathbf{BA} = \mathbf{USV}^{T} = \mathbf{BU'SV}^{T},$$

where $\mathbf{U'} = \mathbf{B}^{-1}\mathbf{U}$. Finally, **A** is rewritten as

$$\mathbf{A} = \mathbf{U'SV}^{T}.$$

Three significant components were extracted from the SVD analysis (see *Results*). The three extracted components of **V** are fitted with double exponential functions as

$$\begin{pmatrix} V1 \\ V2 \\ V3 \end{pmatrix} = \mathbf{C}\begin{pmatrix} 1 \\ \exp(-k_1 t) \\ \exp(-k_2 t) \end{pmatrix},$$

where **C** is a 3 × 3 matrix. According to the time constants obtained, the diffraction profiles of the decomposed components were reconstituted to calculate the difference Fourier maps.

The intensity of each Bragg reflection was estimated by a profile fitting with a Gaussian function. Difference Fourier maps were calculated by using phases and intensity ratios for the overlapping reflections derived from cryoelectron microscopy data (16).

Results

To measure the structural change in the M–N transition of a BR photocycle, we checked the fractional concentration of M and N intermediates. The observable intermediates at the present time resolution and the experimental conditions are limited to M or N (17). The absorption maximum of the unphotolyzed BR is at 570 nm. The absorption of each intermediate state differs from that of unphotolyzed BR. The increase in absorbance at 410 nm and decrease at 570 nm are an indication of deprotonation of the Schiff base, which is characteristic to the M intermediate. The absorbance of the N intermediate is the same as that of the unphotolyzed BR at 410 nm, but lower at 570 nm (17). Fractional concentrations of these intermediate states can therefore be estimated from absorbance changes at 410 nm and 570 nm. Fig. 1*a* shows absorbance changes in wild-type BR (pH 9, 10°C) at 410 nm and 570 nm by a flash excitation. The figure clearly shows that the time course of the absorbance change at 570 nm is different from that at 410 nm. This difference shows the coexistence of M and N intermediates in this process. Fig. 1*b* shows the fractional concentrations of M and N intermediates estimated from the data shown in Fig. 1*a*. Decay kinetics of the M intermediate has two phases (Fig. 1*b*). Because the rate constant of the fast M component is 4.7 sec^{-1}, this component is difficult to detect in a measurement time resolution of longer than 200 ms. The rate constant of the slow M intermediate is 0.91 sec^{-1}, and the rate constant of the N intermediate is 0.27 sec^{-1}. Because the difference between these rate constants is more than 3-fold, it seems easy to separate M and N intermediates in our measurements. It is clear that the M intermediate decays faster than the N intermediate under the present conditions.

In the x-ray diffraction experiments, we used a two-dimensional x-ray detector and an x-ray image intensifier with a cooled CCD camera (15). Because the a and b axes of two-dimensional crystals are not oriented in our samples, a data set consisted of a sequence of two-dimensional ring patterns similar to those in a powder diffraction. The two-dimensional ring patterns obtained by using the detector system were averaged circularly to obtain a series of one-dimensional diffraction profiles. Fig. 2 shows an example of the time-resolved diffraction profiles summed over 16 independent data sets on wild-type BR (pH 9, 10°C).

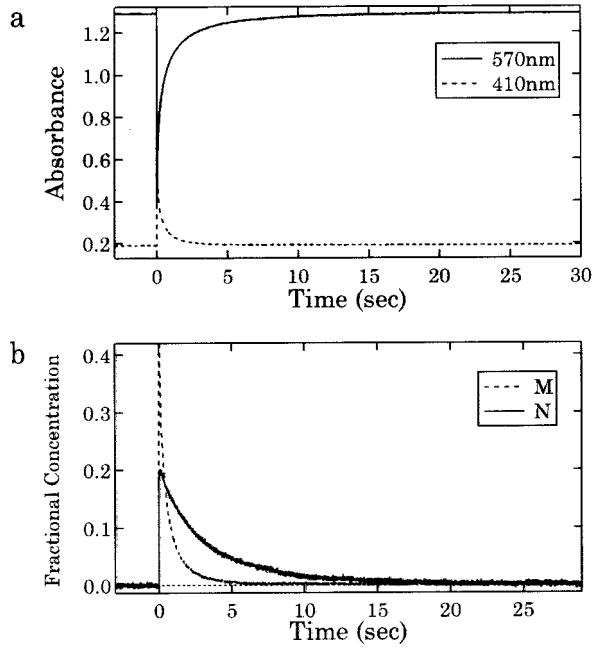

Fig. 1. (*a*) Absorbance changes of wild-type BR (pH 9, 10°C) at 570 nm and 410 nm after a xenon flash lamp excitation. The time resolution is 10 ms. (*b*) Estimated fractional concentrations of M and N intermediates from data shown in *a*. The results of exponential fitting to the fraction concentrations of M and N intermediates were as follows: $f_M(t) = 0.20\exp(-0.91t) + 0.28\exp(-4.7t)$, $f_N(t) = 0.19\exp(-0.27t)$.

We applied SVD treatment to the data shown in Fig. 2 to analyze the decay kinetics of wild-type BR. SVD analysis has been widely used for the characterization of experimental data with various condition parameters (12). In the SVD treatment, we used a weighted data set. The error of the data element $\mathbf{A}(s_i,t_j)$ is given as the square root of the number of incident photons. We treated the error of data **A** depending on s, but not on time, because exposure time is identical for each frame and the intensity changes are small. Vn is the time course of the

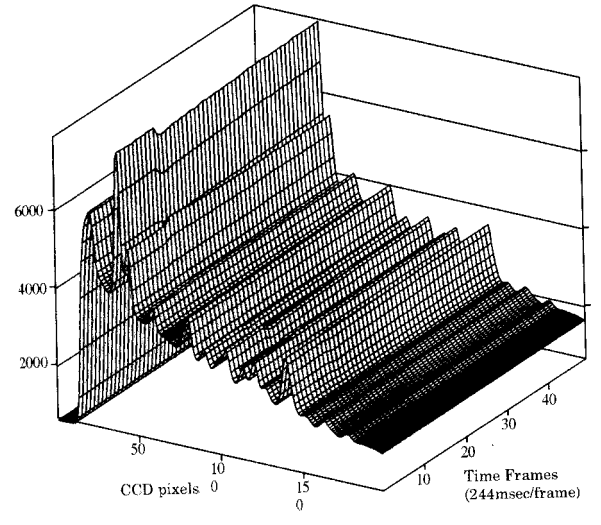

Fig. 2. Time-resolved x-ray diffraction pattern of wild-type BR (pH 9, 10°C) before and after a xenon flash lamp excitation. Bragg peaks up to 7 $Å^{-1}$ are observed. The time resolution of this experiment was 244 ms. Time frames are only shown up to the 50th frame, but diffraction patterns were recorded up to the 200th frame. BR was illuminated at the beginning of the 11th frame.

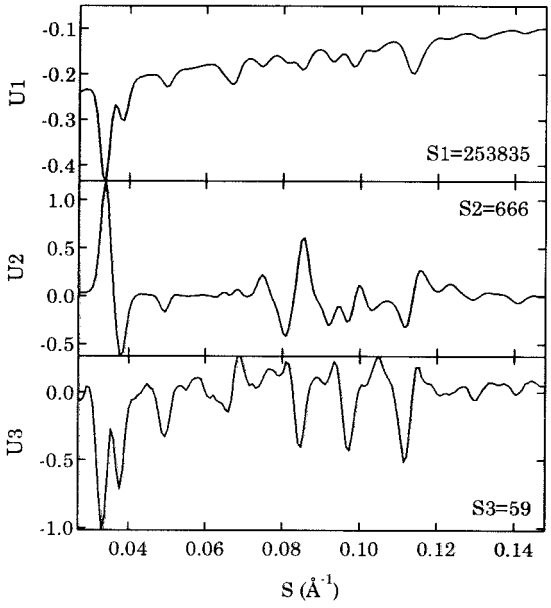

Fig. 3. U spectra of SVD analysis for weighted diffraction data of wild-type BR (pH 9, 10°C). This figure shows 3 major components with their singular values. Singular values of the fourth to eighth components are 33, 27, 26, 25, and 24.

changes in the diffraction pattern, Un. Sn is the magnitude of the *n*th signal. The results of SVD analysis for wild-type BR (pH 9, 10°C) is shown in Fig. 3 and Fig. 4. We can conclude that the first three components are significant based on the results and their singular values. The first component is significant, because of its characteristic, distinct U spectrum and nonzero constant V spectrum. The second two are also significant because of their distinct time dependence shown in their V spectra, and nonrandom characteristic U spectra. On the other hand, the fourth component and higher components are independent of time and

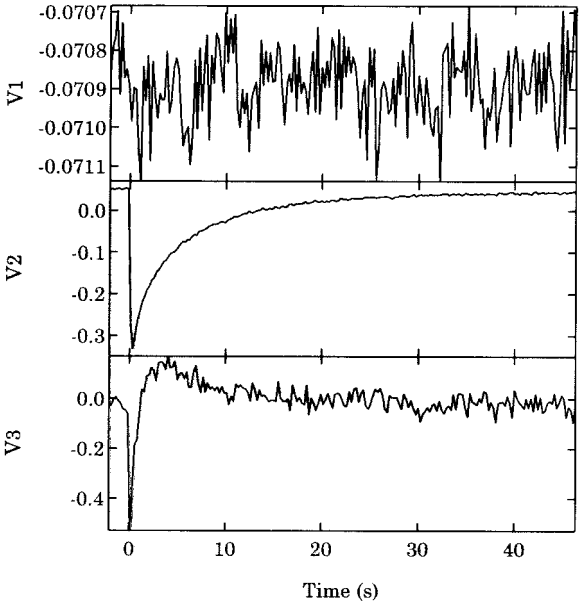

Fig. 4. V spectra of SVD analysis results for weighted diffraction data of wild-type BR (pH 9, 10°C). These spectra indicate the time course of corresponding U spectra.

Table 1. Reconstitution of three components from three basis spectra

Spectra	B0 (constant)	B1 [$k_1 = 0.1322 \pm 0.0010$ (sec^{-1})]	B2 [$k_2 = 0.891 \pm 0.020$ (sec^{-1})]
V1	$-0.070888 \pm 6.7 \times 10^{-6}$		
V2	0.04237 ± 0.00020	-0.2489 ± 0.0016	-0.17941 ± 0.00189
V3	-0.0257 ± 0.0016	0.2820 ± 0.0074	-0.748 ± 0.014

Three V spectra (Fig. 4) were fitted with double exponential functions to extract three components depending on the decay rate. Because V1 has no time dependency, V2 and V3 were fitted with double exponential functions. Each parameter is shown. Three components were extracted from the results: a time-independent component, B0, a slow decay component, B1 (rate constant k_1), and a fast decay component, B2 (rate constant k_2).

fluctuate around 0 (data not shown), indicating that components higher than the fourth component come from noises. The first three singular values are larger than the other values, confirming that the first three components are signals and that the others are noises. U1 is similar to the original diffraction pattern from purple membranes except for its negative sign, which corresponds to the sign of V1. The corresponding V1 shows little time dependence, indicating that U1 does not change during the photocycle. Thus, the first component is mainly composed of the time-independent basic structure of BR. U2 is similar to the difference diffraction profile between the photointermediate and the unphotolyzed state, which has been studied by diffraction methods under photosteady conditions (18). V2, the time dependence of U2, shows a change due to flash excitation at time 0 and decays back to the unphotolyzed state. The third component has a smaller singular value than those of the first and second components but is distinguishable from noises. The existence of the third component indicates that there are at least two different intermediate conformations in the decay process of wild-type BR after a flash excitation. Because the results of absorbance measurements show the existence of M and N intermediates in this time region, two intermediate conformations should be related to these intermediates.

The difference between the M-type (M intermediate) structure and N-type (MN intermediate) structure has been studied by static x-ray diffraction experiments (18). The MN intermediate has been shown to have a deprotonated Schiff base like the M-intermediate, but has an N intermediate-like (N-type) structure (19). According to this report, the intensity ratio of the negative peak of (1 1) reflection to the positive peak of (2 0) reflection is almost 1:1 for the M-type structure, but 1:0 for the N-type structure, under a photosteady state. In the present study, V2 and V3 were found to have negative values at time 0. A few seconds after the flash excitation, V2 remained negative but V3 became positive. Therefore, the intensity ratio of the negative peak of (1 1) reflection to the positive peak of (2 0) reflection shows the existence of an M-like structure just after a flash excitation, but it becomes an N-like structure after a few seconds. This result agrees well with the result of the absorbance measurements (Fig. 1), which indicates that the M intermediate is dominant at first but that the N intermediate becomes dominant after a few seconds.

Because the three components derived from the SVD analysis do not correspond directly to three independent states in the photocycle, we need to reconstitute the diffraction profiles for three states from the three components. Three V spectra were fitted with double exponential functions to decompose into three species depending on the decay rate. Because V1 has no time dependency, V2 and V3 were fitted with double exponential functions to obtain three components: a time-independent component, B0, a decay component, B1 (rate constant $k_1 = 0.132$), and a decay component, B2 (rate constant $k_2 = 0.89$). The rate constants and amplitudes are shown in Table 1. B0 corresponds to a component of the unphotolyzed state that is unchanged during the photocycle, and B1 and B2 are two different components that decay after the flash excitation with different time constants. Just after the flash excitation, the x-ray diffraction profile is a summation of all three profiles, B0, B1, and B2. Absorbance measurements showed that the M intermediate decays fast and the N intermediate decays slowly in wild-type BR (pH 9, 10°C). Then the slow-decay component (B1) mainly comes from the N intermediate and the fast-decay component (B2) from the M intermediate. We analyzed these intensity profiles by the difference Fourier method and estimated the parts of the molecule that showed large changes. In this analysis, we used reflections up to (5 1), and so the maps correspond to 10 Å resolution. Figs. 5 *a* and *b* show the difference electron density maps of wild-type BR calculated from the slow and the fast components, respectively. These figures are electron density differences between the decay components and the unphotolyzed state. Changes near F and G helices are observed for the slow component (Fig. 5*a*), and the positive peak at the outer side of the F helix is higher than the positive peak of the G helix. This is a characteristic property of the N intermediate (9). On the other hand, the positive peak at the outer side of the F helix is similar in height to the positive peak of the G helix (Fig. 5*b*). This indicates that the F helix changes its structure during the M–N transition. This feature is the same as the

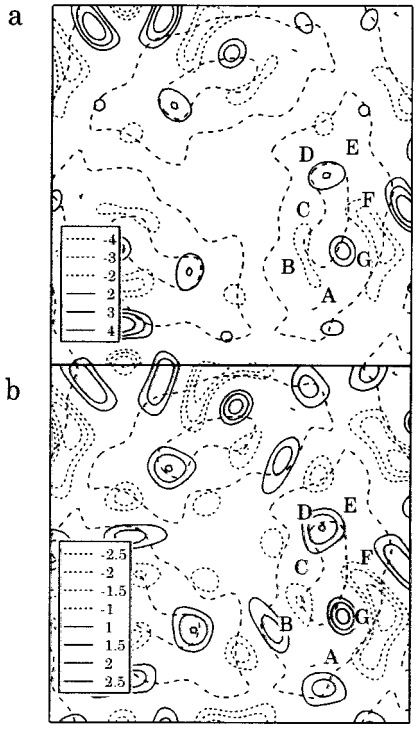

Fig. 5. Difference Fourier maps of the slow and fast components of wild-type BR (pH 9, 10°C) shown in Table 1. (*a*) Map of the slow component (B1). (*b*) Map of the fast component (B2). These are electron density differences between the decay components and the unphotolyzed state. The peak heights of the F and G helices are 5.0 and 3.6 in *a* and 1.9 and 2.3 in *b*, respectively. Estimated errors of these maps are 0.75 and 0.47, respectively.

transition of M-type conformation to N-type conformation in alkaline D96N (18).

Discussion

We measured the structural changes of BR after a flash excitation by time-resolved x-ray diffraction. The only previous time-resolved diffraction study on BR was that by Koch *et al.* (8). They measured the structural decay process of the D96N M intermediate and extracted only one decay component during this process. In the present study, we were able to measure the structural M–N transition of wild-type BR (pH 9, 10°C) as a change in the x-ray diffraction pattern. We used SVD analysis, which has been used frequently in spectroscopy, for analyzing time-resolved x-ray data. This is a powerful method for extracting a small amount of changes from the data (12). We first decomposed the data by SVD analysis and then calculated difference Fourier maps. Considering the noise associated with map calculation, this method is much more effective than decomposition from time-sequential difference Fourier maps. The results of static diffraction studies have shown that the N intermediate structure differed from the M intermediate structure (9, 10). The most prominent difference between these intermediate structures is the change in electron density near the F helix: the change near the F helix is larger in the N intermediate than in the M intermediate. By using electron diffraction with rapid cooling, Subramaniam *et al.* (20) measured the structural changes in intermediate states of wild-type, D96G, and other mutant BR's at various times after excitation. However, they did not observe any differences between the M and N intermediates. Consequently, they concluded that the structural difference between M and N intermediates is trivial. Because clear structural changes in the M–N transition were observed by x-ray diffraction in the present study, our data agree with the results of static experiments showing that BR changes its structure in the M–N transition (9, 10, 18).

We directly observed an increase in electron density at the outer side of the F helix in the M–N transition. This indicates that a part of the F helix moves outward in the M–N transition. In this transition, the Schiff base is reprotonated from D96. D96 is located in a hydrophobic environment and has an unusually high pK, so it is protonated in the unphotolyzed state. This means that pK of D96 needs to decrease for transfer of a proton to the Schiff base. Thus, an important event that lowers the D96 pK is expected to occur in the M–N transition. In this step, structural changes in the cytoplasmic surface of BR were observed by EPR (21, 22). Thorgeirsson *et al.* (22) clearly showed that the EF loop moves in the M–N transition. The result of an electron diffraction experiment also showed that the cytoplasmic end of the F helix is open in the N intermediate (23). The atomic resolution structure of the D96N MN intermediate, which is an N intermediate-like structure, was revealed, but its cytoplasmic side of the F and G helices could not be modeled because of disordering by the movement of these regions (24). This may be explained by movement of the F helix toward neighbors in the crystal lattice being too large to allow all molecules to change conformation simultaneously (23). All these results agree with our results and indicate that the cytoplasmic end of the F helix moves outward extensively in the M–N transition.

The M–N structural transition corresponds to the opening of the proton transfer channel to the cytoplasmic surface. It is thought that this change leads to the introduction of water molecules into the proton channel in the cytoplasmic side and to lowering of the high pK of D96 (18). It facilitates proton transfer from D96 to the retinal Schiff base. This idea is supported by the fact that the M–N transition of the wild-type and the M–MN transition of D96N are influenced by hydration of the samples (18, 25, 26). Replacement of hydrophobic residues located close to the cytoplasmic proton channel, F219, F171, and T46, prolongs the lifetime of the N intermediate. Moreover, T46V and F219L contain an N-like conformer in the unphotolyzed state (20, 27). These residues are located near D96, and the OH group of T46 is hydrogen-bonded to the carboxyl group of D96 (28, 29). These results suggest that perturbation of the environment of D96 stabilizes the hydrogen bond between D96 and neighboring water molecules (30) and prevents the recovery of high pK of D96, which is needed for reprotonation of D96 in the photocycle. If the structural transition from M-type to N-type has the role of introducing water molecule(s) into the proton channel and lowering the D96 pK value, proton transfer from D96 to the Schiff base would occur after this structural transition. Therefore, the MN intermediate may exist in the wild-type photocycle, but it probably decays immediately and is difficult to detect.

We thank Dr. Tatzuo Ueki (Japan Synchrotron Radiation Research Institute) for his support in SPring-8. This work was supported by the SPring-8 Joint Research Promotion Scheme of the Japan Science and Technology Corporation. T.O. is grateful for fellowships from the Japan Society for the Promotion of Science for Japanese Junior Scientists. The x-ray diffraction experiments were performed at SPring-8 (proposal numbers 1997B0146, 1998A0188, and 1999A0347).

1. Jardetzky, O. (1966) *Nature (London)* **211,** 969–970.
2. Dencher, N. A., Dresselhaus, D., Zaccai, G. & Büldt, G. (1989) *Proc. Natl. Acad. Sci. USA* **86,** 7876–7879.
3. Nakasako, M., Kataoka, M., Amemiya, Y. & Tokunaga, F. (1991) *FEBS Lett.* **292,** 73–75.
4. Subramaniam, S., Gerstein, M., Oesterhelt, D. & Henderson, R. (1993) *EMBO J.* **12,** 1–8.
5. Kataoka, M., Kamikubo, H., Tokunaga, F., Brown, L. S., Yamazaki, Y., Maeda, A., Sheves, M., Needleman, R. & Lanyi, J. K. (1994) *J. Mol. Biol.* **243,** 621–638.
6. Brown, L. S., Kamikubo, H., Zimanyi, L., Kataoka, M., Tokunaga, F., Verdegem, P., Lugtenburg, J. & Lanyi, J. K. (1997) *Proc. Natl. Acad. Sci. USA* **94,** 5040–5044.
7. Lanyi, J. K. (1995) *Nature (London)* **375,** 461–463.
8. Koch, M. H. J., Dencher, N. A., Oesterhelt, D., Plöhn, H.-J., Rapp, G. & Büldt, G. (1991) *EMBO J.* **10,** 521–526.
9. Kamikubo, H., Kataoka, M., Váró, G., Oka, T., Tokunaga, F., Needleman, R. & Lanyi, J. K. (1996) *Proc. Natl. Acad. Sci. USA* **93,** 1386–1390.
10. Vonck, J. (1996) *Biochemistry* **35,** 5870–5878.
11. Frankel, R. D. & Forsyth, J. M. (1985) *Biophys. J.* **47,** 387–393.
12. Henry, E. R. & Horfrichter, J. (1992) *Methods Enzymol.* **210,** 129–192.
13. Oesterhelt, D. & Stockenius, W. (1974) *Methods Enzymol.* **31,** 667–678.
14. Fujisawa, T., Inoue, K., Oka, T., Iwamoto, H., Uruga, T., Kumasaka, T., Inoko, Y., Yagi, N., Yamamoto, M. & Ueki, T. (2000) *J. Appl. Cryst.* **33,** 797–800.
15. Amemiya, Y., Ito, K., Yagi, N., Asano, Y., Wakabayashi, K., Ueki, T. & Endo, T. (1995) *Rev. Sci. Instrum.* **66,** 2290–2294.
16. Henderson, R., Baldwin, J. M., Ceska, T. A., Zemlin, F., Beckmann, E. & Downing, K. H. (1990) *J. Mol. Biol.* **213,** 899–929.
17. Váró, G. & Lanyi, J. K. (1991) *Biophys. J.* **59,** 313–322.
18. Kamikubo, H., Oka, T., Imamoto, Y., Tokunaga, F., Lanyi, J. K. & Kataoka, M. (1997) *Biochemistry* **36,** 12282–12287.
19. Sasaki, J., Shichida, Y., Lanyi, J. K. & Maeda, A. (1992) *J. Biol. Chem.* **267,** 20782–20786.
20. Subramaniam, S., Lindahl, M., Bullough, P., Faruqi, A. R., Tittor, J., Oesterhelt, D., Brown, L., Lanyi, J. & Henderson, R. (1999) *J. Mol. Biol.* **287,** 145–161.
21. Steinhoff, H. J., Mollaaghababa, R., Altenbach, C., Hideg, K., Krebs, M., Khorana, H. G. & Hubbell, W. L. (1994) *Science* **266,** 105–107.
22. Thogeirsson, T. E., Xiao, W., Brown, L. S., Needleman, R., Lanyi, J. K. & Shin, Y.-K. (1997) *J. Mol. Biol.* **273,** 951–957.
23. Vonck, J. (2000) *EMBO J.* **19,** 2152–2160.
24. Luecke, H., Schobert, B., Richter, H.-T., Cartailler, J.-P. & Lanyi, J. K. (1999) *Science* **286,** 255–261.
25. Váró, G. & Lanyi, J. K. (1991) *Biochemistry* **30,** 5008–5015.
26. Cao, Y., Váró, G., Chang, M., Ni, B., Needleman, R. & Lanyi, J. K. (1991) *Biochemistry* **30,** 10972–10979.
27. Brown, L. S., Zimanyi, L., Needleman, R., Ottolenghi, M. & Lanyi, J. K. (1993) *Biochemistry* **32,** 7679–7685.
28. Luecke, H., Richter, H.-T. & Lanyi, J. K. (1998) *Science* **280,** 1934–1937.
29. Luecke, H., Schobert, B., Richter, H.-T., Cartailler, J.-P. & Lanyi, J. K. (1999) *J. Mol. Biol.* **291,** 899–911.
30. Yamazaki, Y., Hatanaka, M., Kandori, H., Sasaki, J., Karstens, W. F., Raap, J., Lugtenburg, J., Bizounok, M., Herzfeld, J., Needleman, R., Lanyi, J. K. & Maeda, A. (1995) *Biochemistry* **34,** 7088–7093.